Spatial splay states and splay chimera states in coupled map lattices

Joydeep Singha* and Neelima Gupte†
Department of Physics, Indian Institute of Technology Madras, Chennai, 600036, India
(Received 28 January 2016; published 3 November 2016)

We study the existence and stability of splay states in the coupled sine circle map lattice system using analytic and numerical techniques. The splay states are observed for very low values of the nonlinearity parameter, i.e., for maps which deviate very slightly from the shift map case. We also observe that depending on the parameters of the system the splay state bifurcates to a mixed or chimera splay state consisting of a mixture of splay and synchronized states, together with kinks in the phases of some of the maps and then to a stable globally synchronized state. We show that these pure states and the mixed states are all temporally chaotic for our systems, and we explore the stability of these states to perturbations. Our studies may provide pointers to the behavior of systems in diverse application contexts such as Josephson junction arrays and chemical oscillations.

DOI: 10.1103/PhysRevE.94.052204

I. INTRODUCTION

Extended dynamical systems which model coupled phase oscillators such as the coupled map lattice system [1–5] which we study here show a wide variety of spatiotemporal behavior. The existence of different types of states and their respective dynamics depend largely on the connection topology and the strength of coupling between the individual oscillator sites as well as on the initial condition. Some of the dynamical behavior seen for such systems includes synchronized behavior, spatiotemporally periodic behavior, mixed or chimera states, splay states, and numerous others. In this paper, we discuss the existence and stability of splay states in a coupled map lattice of sine circle maps [3] which is a discrete space, discrete time version of systems of coupled phase oscillators and their bifurcations to a variety of states, including mixed states which we call the splay chimera states.

The splay state, or the antiphase state, is a special type of phase-synchronized state, and is often seen in arrays of coupled phase oscillators. Let $\theta(0),\theta(1),\theta(2),\ldots,\theta(N-1)$ be the phases of N such coupled oscillators. If the phases of the oscillators were to maintain a splay state then the phase of any kth oscillator, $\theta(k)$, is given by $\theta(0)+\frac{2\pi Tk}{N}$, where T denotes the period of the splay state, and $k=0,\ldots,N-1$ [6–12]. Such dynamical states can occur in large numbers. If we have a splay state with N coupled oscillators, then there are $(N-1)!$ equivalent splay states leading to the phenomenon of attractor crowding [13]. If it is possible to switch reliably between these splay states in a physical system, then it can be used as a storage element [14]. A variant of this definition of the splay state has been used in Ref. [15]. This adopted a definition where a splay state is given by $\theta(k)=\theta(0)+2\pi k/N, k=0,\ldots,N-1$, i.e., the phases are evenly distributed around a unit circle. This corresponds to $T=1$ in the former definition. In the present paper, we use this definition of Refs. [15–17] as our definition of the splay state and call these states "spatial splay states" to distinguish them from the earlier definition.

As mentioned above, coupled phase oscillator arrays exhibit a variety of pure states, such as the synchronized and splay states. In addition, they can also exhibit a variety of chimera states or mixed states, e.g., chimera states with phase synchronized and phase desynchronized subgroups of oscillators have been observed in phase oscillator arrays with continuous time evolution [18–20]. Here we discuss the existence and stability of spatial splay states as well as splay chimera states in a system of coupled sine circle maps. The splay chimera states seen here are mixed states in which the phases of some of the maps of the system show a splay-like diagonal structure, and others show phase synchronized and phase jump behavior.

We note that pure splay states have been observed in laboratory systems like arrays of coupled Josephson junctions, coupled multimode laser systems, and coupled Staurt-Landau oscillators. The stability of such states has been studied in coupled Josephson junction arrays [6–9]. Splay states have been found to be neutrally stable in the presence of a purely resistive load [6,7] and have been found to be stable states with purely capacitive loads [8]. Strogatz and Mirollo gave an exact theory that explained this neutral stability [10]. Nichols and Wiesenfield have shown analytically, that if $N\to\infty$, splay states can become attracting or repelling or neutrally stable depending on the coupling and the conductance term in the governing equations [9]. In an array of globally pulse-coupled rotators pure splay states are found to marginally stable [11]. The application of such states in general to beam steering [21] and beam forming in the context of repulsively coupled Stuart-Landau oscillators was discussed [22]. In delay coupled Stuart-Landau systems, the stabilization of splay states was achieved using the speed gradient method from control theory [12].

As mentioned above, we study the splay states and splay chimera states in the context of a system of coupled sine circle maps, a model for a system of oscillators. A diffusively coupled system of sine circle maps has been studied in Ref. [23]. Coupled map lattice systems where time and space are discrete, but map variables are continuous, have always been considered useful models of extended systems, as they are analytically and computationally more tractable than continuous flows but retain the complexity and variety which can be found in their solutions. Chimera states of different kinds have already

*joydeep@physics.iitm.ac.in
†gupte@physics.iitm.ac.in

been observed in coupled map lattice systems [3–5]. We show here that a sine circle map CML with two groups of maps sharing a global coupling can show pure spatial splay states which bifurcate to mixed states with increasing strength of nonlinearity in the individual maps. In the presence of even higher nonlinearity, these mixed states bifurcate to globally synchronized states. We also study the temporal behavior of the system and find that it is chaotic in nature as well as the sensitivity of the system to perturbations.

Our paper is organized in the following manner: Sec. II discusses the model and form of coupling, which is global coupling for a system with two subgroups, and distinct values of intragroup and intergroup coupling. Section III discusses the spatial splay states and their temporal fixed points and stability, as well as multiple copy spatial splay states and their stability. The Gershgorin circle theorem is used to find the bounds on the eigen-values, and these are compared with numerically obtained eigenvalues. We discuss the temporal behavior of the two-copy spatial splay states in Sec. IV A, using Lyapunov exponents and the order parameter as our tools of analysis. Section IV B discusses the bifurcation behavior of the splay states, mixed states are discussed in Sec. IV C, and the stability of the spatial splay state to perturbation is discussed in Sec. IV D. Section V summarizes our conclusions. We utilize several theorems from linear algebra for our stability analysis. These are summarized in Appendix A. We also discuss the stability of the k-copy splay state in Appendix B.

II. THE MODEL

We use a globally coupled sine circle map lattice system with two groups of maps, in which all elements in one group are coupled to each other with a given coupling strength, and to all the elements in the other group with another coupling strength [3]. Each single sine circle map [24] evolves by the equation

$$\theta_{n+1} = \theta_n + \Omega - \frac{K}{2\pi}\sin(2\pi\theta_n) \mod 1, \tag{1}$$

where Ω is the frequency ratio parameter in the absence of nonlinearity and K determines the strength of the nonlinearity. This map shows Arnold tongues organized by frequency locking and quasiperiodic behavior [25]. Physical systems where behavior similar to frequency locking and quasiperiodicity in the circle map is seen, are forced Rayleigh-Benard convection [26], cardiac cells, and biological models [27]. The single map shows universality in mode-locking structure prior to both period doubling routes to chaos, and quasiperiodic routes to chaos [24,25] depending on the value of Ω. The evolution equation for the globally coupled CML model with two distinct groups of maps is given by [3]

$$\theta^{\sigma}_{n+1}(i) = \theta^{\sigma}_{n}(i) + \Omega - \frac{K}{2\pi}\sin\left[2\pi\theta^{\sigma}_{n}(i)\right] + \sum_{\sigma'=1}^{2}\frac{\epsilon_{\sigma\sigma'}}{N_{\sigma'}} \times \left(\sum_{j=1}^{N_{\sigma'}}\left\{\theta^{\sigma'}_{n}(i) + \Omega - \frac{K}{2\pi}\sin\left[2\pi\theta^{\sigma'}_{n}(i)\right]\right\}\right) \mod 1. \tag{2}$$

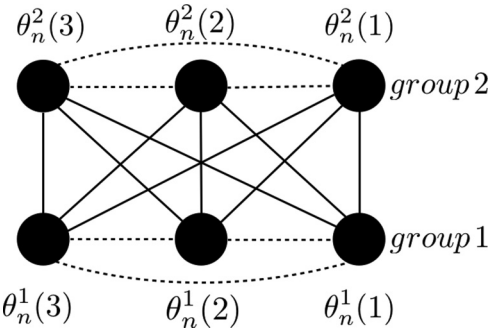

FIG. 1. The diagram above illustrates the connection scheme of the globally connected network. The black dots represent the maps in each group with three maps in each group. Each map in the system is coupled to the maps in its own group via a coupling ϵ_1 (represented by dotted edges) and to the maps in the other group via a coupling ϵ_2 (represented by solid edges).

This equation defines the evolution of the ith map in the group σ, where σ takes values 1, 2, and N_σ is the number of maps in the group σ. We also define the coupling parameters to be $\epsilon_{11} = \epsilon_{22} = \epsilon_1$ and $\epsilon_{12} = \epsilon_{21} = \epsilon_2$ where $\epsilon_1 + \epsilon_2 = 1$. Thus, our model consists of two groups of identical sine circle maps with N_σ being the number of maps in the group σ. Each map in a group is coupled to all the maps in the its own group by the parameter ϵ_1, whereas it is coupled to the maps in the other group by the parameter ϵ_2 (Fig. 1). Thus the system of Eq. (2) is controlled by three independent parameters, K, Ω, ϵ_1.

Chimera states, where the phases of maps in one group are all synchronized, and the phases in the other group are all desynchronized, have been observed as solutions of Eq. (2) [3] on evolution from an initial condition where one of the groups were assigned constant phases and the phases of the maps in the other group were assigned randomly values between 0 and 1. For the same initial condition it was found that clustered chimera states exist in the system. We note that high-dimensional dynamical systems, such as the one under study, are multiattractor systems and are strongly sensitive to different classes of initial conditions [23]. We hence examine the evolution of Eq. (2) with a class of initial conditions which is completely distinct from those of Ref. [3] and hence results in a distinct class of spatiotemporal behavior.

In this paper, we use an initial condition where the entire system of $2N$ lattice sites supports a single spatial splay state where the phase difference between any two consecutive maps is given by $\frac{1}{2N}$. If we iterate Eq. (2), using this initial condition; the single spatial splay state is destabilized and breaks into two identical spatial splay states for low values of K, i.e., low nonlinearity. The phases of the maps in each of the group are such that they separately constitute splay states which are exact copies of each other. Thus the initial splay state settles down to a period 2 splay state. The two states are shown in Fig. 2(a) and Fig. 2(b).

We note that the spatial splay states can have a variety of temporal behaviors. Hence, when we use the term splay states in the subsequent discussion, we mean that their spatial structure is splay, i.e., the phase angles are uniformly distributed over a circle. Their temporal behavior is discussed separately in each context.

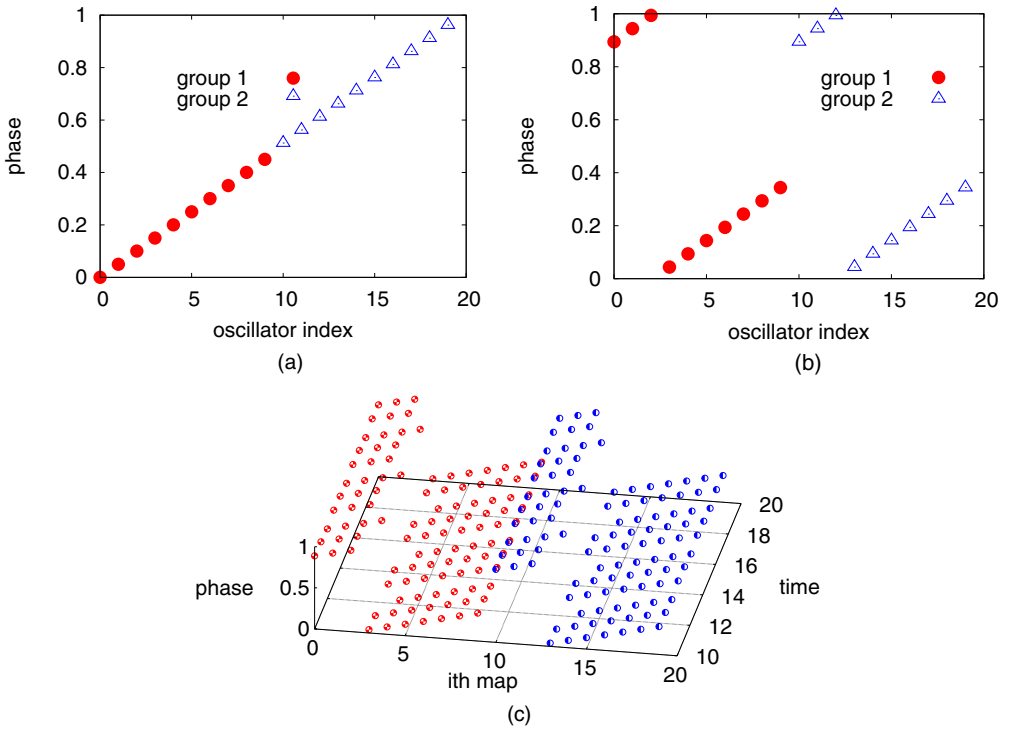

FIG. 2. (a) We plot an initial condition, a spatial splay state throughout the system where the difference between the phases of two consecutive maps is $\frac{1}{20}$, where the system has 20 maps, with 10 maps in each subgroup. This initial condition for (b) for $K = 10^{-10}$, $\Omega = \frac{2}{7}, \epsilon_1 = 0.01$ evolves to a spatial splay state with two copies. The phase difference between any two consecutive maps of each copy is given by $\frac{1}{20}$. The phase difference between the last map of group 1 and the first map of group 2 is 0.55. (c) A space time plot of the above state.

III. STABILITY ANALYSIS OF SPATIAL SPLAY STATES

Consider the evolution equation (2). We examine the condition for a frozen spatial splay state for this equation.

A. Fixed points

Let the phases of the maps for a single splay state spanning the $2N$ lattice sites be $\theta_s^1(0) = 0$, $\theta_s^1(1) = \frac{1}{2N}$, $\theta_s^1(2) = \frac{2}{2N}, \ldots,$ $\theta_s^1(N-1) = \frac{N-1}{2N}$, $\theta_s^2(0) = \frac{N}{2N}, \ldots,$ $\theta_s^2(N-1) = \frac{2N-1}{2N}$. For these phases to be frozen in time we must have

$$\theta_s^\sigma(i) = \theta_s^\sigma(i) + \Omega - \frac{K}{2\pi}\sin\left[2\pi\theta_s^\sigma(i)\right] + \sum_{\sigma'=1}^{2}\frac{\epsilon_{\sigma\sigma'}}{N_{\sigma'}} \times\left(\sum_{j=1}^{N_{\sigma'}}\left\{\theta_s^{\sigma'}(i) + \Omega - \frac{K}{2\pi}\sin\left[2\pi\theta_s^{\sigma'}(i)\right]\right\}\right) \mod 1 \tag{3}$$

or

$$\frac{K}{2\pi}\sin\left[2\pi\theta_s^\sigma(i)\right] = \Omega + \sum_{\sigma'=1}^{2}\frac{\epsilon_{\sigma\sigma'}}{N_{\sigma'}}\left(\sum_{j=1}^{N_{\sigma'}}\left\{\theta_s^{\sigma'} + \Omega - \frac{K}{2\pi}\sin\left[2\pi\theta_s^{\sigma'}(i)\right]\right\}\right) - q_i^\sigma. \tag{4}$$

Here q_i^σ is an integer, which can differ for different values of i and σ. For any two maps in a given group σ we can write

$$\frac{K}{2\pi}\left[\sin 2\pi\theta_s^\sigma(i) - \sin 2\pi\theta_s^\sigma(j)\right] = q_j^\sigma - q_i^\sigma. \tag{5}$$

The right-hand side of Eq. (5), i.e., $q_j^\sigma - q_i^\sigma$, can take values $0, \pm1, \pm2, \ldots$. The quantity $[\sin 2\pi\theta_s^\sigma(i) - \sin 2\pi\theta_s^\sigma(j)]$ on the left-hand side of the same equation can have values within the bounded set, $[-2,2]$, and the maximum value of K is 1. So the left-hand side of Eq. (5) can take values only from the bounded set, $[-\frac{1}{\pi}, \frac{1}{\pi}]$. Thus, the only possible value of $q_j^\sigma - q_i^\sigma$ is 0, which implies $q_0^1 = q_1^1 = \cdots = q_{N-1}^1 = q^1$ and $q_0^2 = q_1^2 = \cdots = q_{N-1}^2 = q^2$. This implies that for nonzero values of K the only possible solution that can be frozen in time is when all the maps in a group are synchronized, i.e., all the maps in the group have equal phases. Hence, a single spatial splay state which spans all the sites and is frozen in time can exist only when $K = 0$, i.e., for shift maps. For $K = 0$, Eq. (4) takes the form

$$\Omega + \sum_{\sigma'=1}^{2}\frac{\epsilon_{\sigma\sigma'}}{N_{\sigma'}}\left[\sum_{j=1}^{N_{\sigma'}}\left(\theta_s^{\sigma'} + \Omega\right)\right] = q_i^\sigma. \tag{6}$$

If we substitute the phases for the single spatial splay state in the above equation, then we have for group 1,

$$2\Omega + \frac{3N-1}{4N} - \frac{\epsilon_1}{2} = q^1. \tag{7}$$

For group 2,

$$2\Omega + \frac{N-1}{4N} + \frac{\epsilon_1}{2} = q^2. \tag{8}$$

Solving Eqs. (7) and (8) and for Ω, ϵ_1 we have

$$\Omega = \frac{q^1 + q^2}{4} - \frac{2N-1}{8N}, \tag{9}$$

$$\epsilon_1 = q^2 - q^1 + \frac{1}{2}. \tag{10}$$

As we have restricted the values of ϵ_1, Ω to [0,1], from equation Eq. (10) we find that $q^2 - q^1 = 0$, so that $\epsilon_1 = \frac{1}{2}$. If we choose $q^1 = q^2 = 1,2$, then the values of Ω remain within [0,1]. So the single, system wide, spatial splay state can be frozen in time for two sets of parameter values for a given N. These are $K = 0$, $\epsilon_1 = 0.5$, $\Omega = 0.5 - \frac{2N-1}{8N}, 1 - \frac{2N-1}{8N}$.

B. Stability matrix

We now examine the stability of the solutions of Eq. (2). Here we set up the stability matrix of the system. The general form of the Jacobian for the evolution equation (2) at any time step is a $2N \times 2N$ matrix and is given by

$$J = \begin{bmatrix} A & B \\ C & D \end{bmatrix}. \tag{11}$$

Here A, B, C, D are matrices of order $N \times N$:

$$A = \begin{bmatrix} \left(2 - \frac{N-1}{N}\epsilon_1 - \epsilon_2\right) f'\left[\theta_n^1(1)\right] & \frac{\epsilon_1}{N} f'\left[\theta_n^1(2)\right] & \cdots & \frac{\epsilon_1}{N} f'\left[\theta_n^1(N)\right] \\ \frac{\epsilon_1}{N} f'\left[\theta_n^1(1)\right] & \left(2 - \frac{N-1}{N}\epsilon_1 - \epsilon_2\right) f'\left[\theta_n^1(2)\right] & \cdots & \frac{\epsilon_1}{N} f'\left[\theta_n^1(N)\right] \\ \cdots & \cdots & \cdots & \cdots \\ \frac{\epsilon_1}{N} f'\left[\theta_N^1(1)\right] & \frac{\epsilon_1}{N} f'\left[\theta_N^1(2)\right] & \cdots & \left(2 - \frac{N-1}{N}\epsilon_1 - \epsilon_2\right) f'\left[\theta_N^1(N)\right] \end{bmatrix}, \tag{12}$$

$$D = \begin{bmatrix} \left(2 - \frac{N-1}{N}\epsilon_1 - \epsilon_2\right) g'\left[\theta_n^2(1)\right] & \frac{\epsilon_1}{N} g'\left[\theta_n^2(2)\right] & \cdots & \frac{\epsilon_1}{N} g'\left[\theta_n^2(N)\right] \\ \frac{\epsilon_1}{N} g'\left[\theta_n^2(1)\right] & \left(2 - \frac{N-1}{N}\epsilon_1 - \epsilon_2\right) g'\left[\theta_n^2(2)\right] & \cdots & \frac{\epsilon_1}{N} g'\left[\theta_n^2(N)\right] \\ \cdots & \cdots & \cdots & \cdots \\ \frac{\epsilon_1}{N} g'\left[\theta_N^2(1)\right] & \frac{\epsilon_1}{N} g'\left[\theta_N^2(2)\right] & \cdots & \left(2 - \frac{N-1}{N}\epsilon_1 - \epsilon_2\right) g'\left[\theta_N^2(N)\right] \end{bmatrix}, \tag{13}$$

$$B = \begin{bmatrix} \frac{\epsilon_2}{N} g'\left[\theta_n^2(1)\right] & \frac{\epsilon_2}{N} g'\left[\theta_n^2(2)\right] & \cdots & \frac{\epsilon_2}{N} g'\left[\theta_n^2(N)\right] \\ \frac{\epsilon_2}{N} g'\left[\theta_n^2(1)\right] & \frac{\epsilon_2}{N} g'\left[\theta_n^2(2)\right] & \cdots & \frac{\epsilon_2}{N} g'\left[\theta_n^2(N)\right] \\ \cdots & \cdots & \cdots & \cdots \\ \frac{\epsilon_2}{N} g'\left[\theta_n^2(1)\right] & \frac{\epsilon_2}{N} g'\left[\theta_n^2(2)\right] & \cdots & \frac{\epsilon_2}{N} g'\left[\theta_n^2(N)\right] \end{bmatrix}, \tag{14}$$

$$C = \begin{bmatrix} \frac{\epsilon_2}{N} f'\left[\theta_n^2(1)\right] & \frac{\epsilon_2}{N} f'\left[\theta_n^2(2)\right] & \cdots & \frac{\epsilon_2}{N} f'\left[\theta_n^2(N)\right] \\ \frac{\epsilon_2}{N} f'\left[\theta_n^2(1)\right] & \frac{\epsilon_2}{N} f'\left[\theta_n^2(2)\right] & \cdots & \frac{\epsilon_2}{N} f'\left[\theta_n^2(N)\right] \\ \cdots & \cdots & \cdots & \cdots \\ \frac{\epsilon_2}{N} f'\left[\theta_n^2(1)\right] & \frac{\epsilon_2}{N} f'\left[\theta_n^2(2)\right] & \cdots & \frac{\epsilon_2}{N} f'\left[\theta_n^2(N)\right] \end{bmatrix}, \tag{15}$$

where $f'[\theta_n^1(j)] = 1 - K\cos[2\pi\theta_N^1(j)]$ and $g'[\theta_n^2(j)] = 1 - K\cos[2\pi\theta_N^2(j)]$. If we substitute the value $K = 0$ in the Jacobian of Eq. (11), then it has the form

$$J_S = \begin{bmatrix} A & B \\ B & A \end{bmatrix}, \tag{16}$$

where

$$A = \begin{bmatrix} \left(1 + \frac{\epsilon_1}{N}\right) & \frac{\epsilon_1}{N} & \cdots & \frac{\epsilon_1}{N} \\ \frac{\epsilon_1}{N} & \left(1 + \frac{\epsilon_1}{N}\right) & \cdots & \frac{\epsilon_1}{N} \\ \cdots & \cdots & \cdots & \cdots \\ \frac{\epsilon_1}{N} & \frac{\epsilon_1}{N} & \cdots & \left(1 + \frac{\epsilon_1}{N}\right) \end{bmatrix}, \tag{17}$$

$$B = \begin{bmatrix} \frac{\epsilon_2}{N} & \frac{\epsilon_2}{N} & \cdots & \frac{\epsilon_2}{N} \\ \frac{\epsilon_2}{N} & \frac{\epsilon_2}{N} & \cdots & \frac{\epsilon_2}{N} \\ \cdots & \cdots & \cdots & \cdots \\ \frac{\epsilon_2}{N} & \frac{\epsilon_2}{N} & \cdots & \frac{\epsilon_2}{N} \end{bmatrix}. \tag{18}$$

The matrix J_S [Eq. (16)] is a block circulant matrix [28]. We can block diagonalize it using a matrix $\mathbf{P}$ whose form [28,29] is given by

$$\mathbf{P} = F_2 \otimes I_N, \tag{19}$$

where I_N is a $N \times N$ identity matrix and F_2 is a 2×2 Fourier matrix [28] which is of the form

$$F_2 = \frac{1}{\sqrt{2}} \begin{bmatrix} 1 & 1 \\ 1 & \omega \end{bmatrix} \tag{20}$$

with $\omega = \exp(\frac{2\pi i}{2}) = \cos\pi + i\sin\pi = -1$. So we have

$$\mathbf{P}^{-1} J_S \mathbf{P} = J_S^* = \begin{bmatrix} A + B & 0 \\ 0 & A - B \end{bmatrix}, \tag{21}$$

where

$$A + B = \begin{bmatrix} \left(1 + \frac{\epsilon_1+\epsilon_2}{N}\right) & \frac{\epsilon_1+\epsilon_2}{N} & \cdots & \frac{\epsilon_1+\epsilon_2}{N} \\ \frac{\epsilon_1+\epsilon_2}{N} & \left(1 + \frac{\epsilon_1+\epsilon_2}{N}\right) & \cdots & \frac{\epsilon_1+\epsilon_2}{N} \\ \cdots & \cdots & \cdots & \cdots \\ \frac{\epsilon_1+\epsilon_2}{N} & \frac{\epsilon_1+\epsilon_2}{N} & \cdots & \left(1 + \frac{\epsilon_1+\epsilon_2}{N}\right) \end{bmatrix}, \tag{22}$$

$$A-B=\begin{bmatrix}\left(1+\frac{\epsilon_1-\epsilon_2}{N}\right) & \frac{\epsilon_1-\epsilon_2}{N} & \cdots & \frac{\epsilon_1-\epsilon_2}{N}\\ \frac{\epsilon_1-\epsilon_2}{N} & \left(1+\frac{\epsilon_1-\epsilon_2}{N}\right) & \cdots & \frac{\epsilon_1-\epsilon_2}{N}\\ \cdots & \cdots & \cdots & \cdots\\ \frac{\epsilon_1-\epsilon_2}{N} & \frac{\epsilon_1-\epsilon_2}{N} & \cdots & \left(1+\frac{\epsilon_1-\epsilon_2}{N}\right)\end{bmatrix}, \tag{23}$$

$A+B$ and $A-B$ are block circulant matrices [28]. The jth eigenvalue λ_j of the matrix $A+B$ and $A-B$ is given by

$$\lambda_j^{A\pm B}=1+\frac{\epsilon_1\pm\epsilon_2}{N}+\frac{\omega^j(\epsilon_1\pm\epsilon_2)}{N}+\frac{\omega^{2j}(\epsilon_1\pm\epsilon_2)}{N}+\cdots+\frac{\omega^{(N-1)j}(\epsilon_1\pm\epsilon_2)}{N}, \tag{24}$$

where ω is the Nth root of unity, i.e., $\omega=\exp(\frac{2\pi i}{N})$

Setting $j=0$ we obtain the zeroth eigenvalues of the matrices $A+B$, $A-B$. So,

$$\begin{aligned}\lambda_0^{A+B}&=1+\frac{\epsilon_1+\epsilon_2}{N}\times N\\&=1+\epsilon_1+\epsilon_2\\&=2,\\ \lambda_0^{A-B}&=1+\frac{\epsilon_1-\epsilon_2}{N}\times N\\&=1+\epsilon_1-\epsilon_2\\&=2\epsilon_1.\end{aligned}$$

For any $j>0$ we have

$$\begin{aligned}\lambda_j^{A\pm B}&=1+\frac{\epsilon_1\pm\epsilon_2}{N}(1+\omega^j+\omega^{2j}+\cdots+\omega^{(N-1)j})\\&=1,\end{aligned}$$

where we use $\epsilon_1+\epsilon_2=1$ and a property of the Nth root of unity. So the eigenvalues of the matrix J_S^* for $K=0$, are 2, $2\epsilon_1$, and $2N-2$ fold degenerate eigenvalues 1. For $\epsilon_1=0.5$ the eigenvalues are 2, and the $2N-1$-fold degenerate eigenvalues 1. As the Jacobian [Eq. (11)] does not depend on Ω, the eigenvalues are same for both sets of parameter values at which the single system wide spatial splay states are frozen in time. Hence, for our system the frozen single spatial splay state is unstable in one direction, and neutrally stable in all the other directions in the phase space. We note that an initial condition, which is a single splay state over the $2N$ sites, did not evolve to a frozen spatial splay state in any of our simulations. However, we do find that this initial condition evolves to two copies of a spatial splay state for several parameter values. Figure 2 shows the phase diagram of the system in the space of parameters Ω, ϵ_1 evolved with an initial condition which is a single splay state. The parameter space is divided into a 100×100 grid and each initial condition is evolved for 1.5×10^6 iterates at every grid point, and the phase configuration of system 2 is checked with an accuracy of 10^{-4}. In Fig. 3(a) we show the phase diagram in Ω,ϵ_1 space for $K=0$. Here 32.91% of the total area of Fig. 3(a) (with an accuracy 10^{-4}) is occupied by the two-copy splay states [Fig. 2(b). If we set the value of K to 10^{-8}, with the same accuracy, 32.11% of the total area of the phase diagram in Fig. 3(b) corresponds to the two-copy splay states. Figures 3(a) and 3(b) clearly show that a large portion of the Ω,ϵ_1 space contains the two-copy splay states which evolve from an initial condition where the phase difference between any two consecutive map was $1/2N$ [Fig. 2(a)] using Eq. (2). At the boundary of this region the two-copy splay states bifurcate to the phase slipped states due to the change in parameters Ω, ϵ_1. See Fig. 3(c) where two-copy splay states with a phase slip between group 1 and group 2 are shown. We discuss the stability of the two-copy splay state in the next section.

C. Two-copy spatial splay states

Here we analyze the stability of the two-copy spatial splay state. Let the phases of the maps in the system for a two-copy splay state be $\theta_n^1(0)$, $\theta_n^1(1)$, $\theta_n^1(2),\ldots,\theta_n^1(N-1)$, $\theta_n^2(0)$, $\theta_n^2(1)$, $\theta_n^2(2),\ldots,\theta_n^2(N-1)$ with $\theta_n^1(i)-\theta_n^1(i+1)=\frac{1}{2N}$, $\theta_n^2(i)-\theta_n^2(i+1)=\frac{1}{2N}$, and $\theta_n^1(0)=\theta_n^2(0)$. The Jacobian matrix of the system can be reduced to a simpler form as in the previous subsection and the bounds on the eigenvalues can be obtained. Since we have two identical splay states, constituted by the maps in each group, let us rewrite phases of the maps in any one of them as $\theta(0)$, $\theta(1)$, $\theta(2),\ldots,\theta(N-1)$ where $\theta(i)-\theta(i+1)=\frac{1}{2N}$. Then the Jacobian [Eq. (11)] takes the form

$$J_{2S}=\begin{bmatrix}C & D\\ D & C\end{bmatrix}, \tag{25}$$

where

$$C=\begin{bmatrix}\left(1+\frac{\epsilon_1}{N}\right)[1-K\cos2\pi\theta_n(0)] & \frac{\epsilon_1}{N}[1-K\cos2\pi\theta_n(1)] & \cdots & \frac{\epsilon_1}{N}[1-K\cos2\pi\theta_n(N-1)]\\ \frac{\epsilon_1}{N}[1-K\cos2\pi\theta_n(0)] & \left(1+\frac{\epsilon_1}{N}\right)[1-K\cos2\pi\theta_n(1)] & \cdots & \frac{\epsilon_1}{N}[1-K\cos2\pi\theta_n(N-1)]\\ \cdots & \cdots & \cdots & \cdots\\ \frac{\epsilon_1}{N}[1-K\cos2\pi\theta_n(0)] & \frac{\epsilon_1}{N}[1-K\cos2\pi\theta_n(1)] & \cdots & \left(1+\frac{\epsilon_1}{N}\right)[1+K\cos2\pi\theta_n(N-1)]\end{bmatrix}, \tag{26}$$

$$D=\begin{bmatrix}\frac{\epsilon_2}{N}[1-K\cos2\pi\theta_n(0)] & \frac{\epsilon_2}{N}[1-K\cos2\pi\theta_n(1)] & \cdots & \frac{\epsilon_2}{N}[1-K\cos2\pi\theta_n(N-1)]\\ \frac{\epsilon_2}{N}[1-K\cos2\pi\theta_n(0)] & \frac{\epsilon_2}{N}[1-K\cos2\pi\theta_n(1)] & \cdots & \frac{\epsilon_2}{N}[1-K\cos2\pi\theta_n(N-1)]\\ \cdots & \cdots & \cdots & \cdots\\ \frac{\epsilon_2}{N}[1-K\cos2\pi\theta_n(0)] & \frac{\epsilon_2}{N}[1-K\cos2\pi\theta_n(1)] & \cdots & \frac{\epsilon_2}{N}[1-K\cos2\pi\theta_n(N-1)]\end{bmatrix}. \tag{27}$$

The matrix J_{2S} [Eq. (25)] is also a block circulant matrix [28]. We can again block diagonalize it using $\mathbf{P}$,

$$\mathbf{P}^{-1}J_{2S}\mathbf{P}=J_{2S}^*=\begin{bmatrix}C+D & 0\\ 0 & C-D\end{bmatrix}, \tag{28}$$

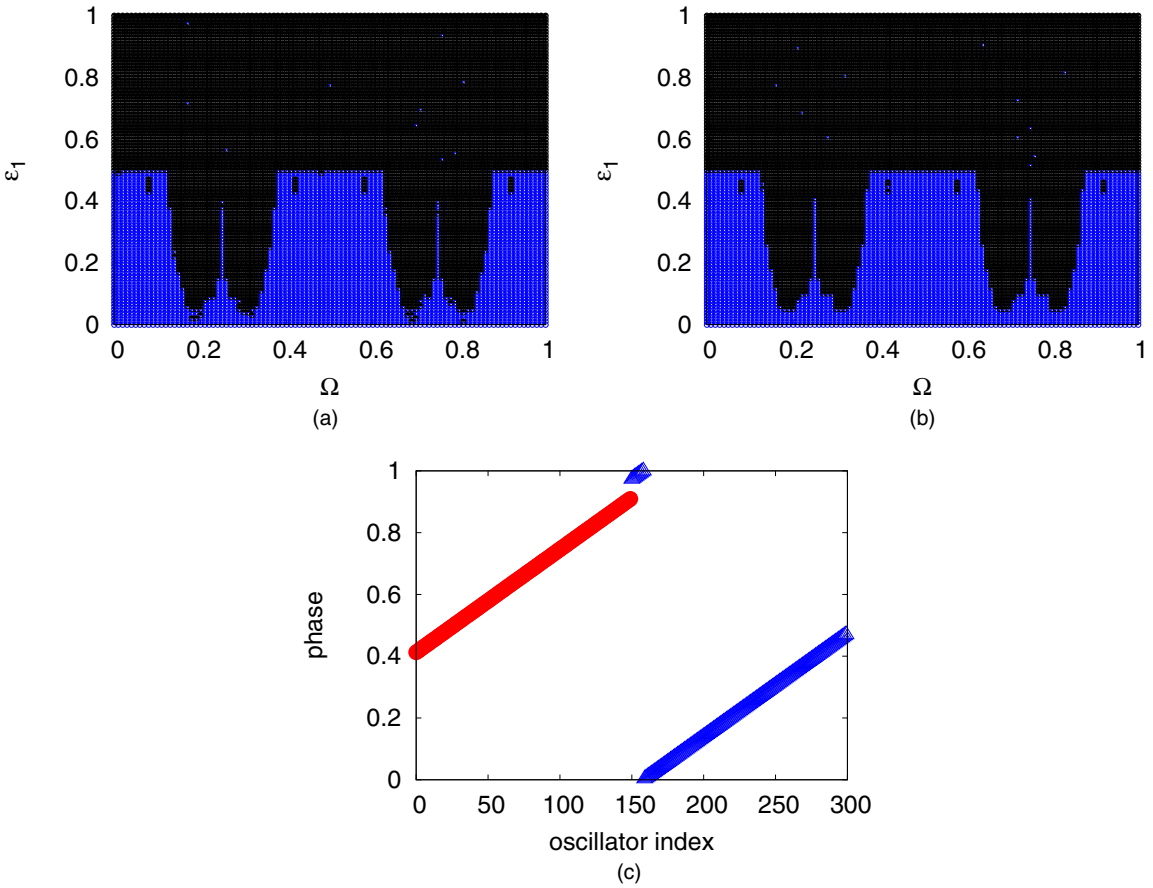

FIG. 3. The phase diagram in the Ω, ϵ_1 space of the states obtained from the evolution of a single splay state at the values (a) $K = 0.0$, (b) $K = 10^{(-8)}$. The blue circles denote the two-copy splay states as in Fig. 2(b), and the black circles denote two-copy splay states with a phase slip between the last map of the first group and the first map of the second group. The spatial splay nature is maintained within each group. (c) Two-copy splay states with a phase slip between group (1) and group (2) are shown for the parameter values, $K = 0.0$, $\Omega = 0.04$, $\epsilon_1 = 0.67$.

where

$$C + D = \begin{bmatrix} \left(1 + \frac{\epsilon_1+\epsilon_2}{N}\right)[1 - K\cos 2\pi\theta(0)] & \frac{\epsilon_1+\epsilon_2}{N}[1 - K\cos 2\pi\theta(1)] & \cdots & \frac{\epsilon_1+\epsilon_2}{N}[1 - K\cos 2\pi\theta(N-1)] \\ \frac{\epsilon_1+\epsilon_2}{N}[1 - K\cos 2\pi\theta(0)] & \left(1 + \frac{\epsilon_1+\epsilon_2}{N}\right)[1 - K\cos 2\pi\theta(1)] & \cdots & \frac{\epsilon_1+\epsilon_2}{N}[1 - K\cos 2\pi\theta(N-1)] \\ \cdots & \cdots & \cdots & \cdots \\ \frac{\epsilon_1+\epsilon_2}{N}[1 - K\cos 2\pi\theta(0)] & \frac{\epsilon_1+\epsilon_2}{N}[1 - K\cos 2\pi\theta(1)] & \cdots & \left(1 + \frac{\epsilon_1+\epsilon_2}{N}\right)[1 - K\cos 2\pi\theta(N-1)] \end{bmatrix}, \tag{29}$$

$$C - D = \begin{bmatrix} \left(1 + \frac{\epsilon_1-\epsilon_2}{N}\right)[1 - K\cos 2\pi\theta(0)] & \frac{\epsilon_1-\epsilon_2}{N}[1 - K\cos 2\pi\theta(1)] & \cdots & \frac{\epsilon_1-\epsilon_2}{N}[1 - K\cos 2\pi\theta(N-1)] \\ \frac{\epsilon_1-\epsilon_2}{N}[1 - K\cos 2\pi\theta(0)] & \left(1 + \frac{\epsilon_1-\epsilon_2}{N}\right)[1 - K\cos 2\pi\theta(1)] & \cdots & \frac{\epsilon_1-\epsilon_2}{N}[1 - K\cos 2\pi\theta(N-1)] \\ \cdots & \cdots & \cdots & \cdots \\ \frac{\epsilon_1-\epsilon_2}{N}[1 - K\cos 2\pi\theta(0)] & \frac{\epsilon_1-\epsilon_2}{N}[1 - K\cos 2\pi\theta(1)] & \cdots & \left(1 + \frac{\epsilon_1-\epsilon_2}{N}\right)[1 - K\cos 2\pi\theta(N-1)] \end{bmatrix}. \tag{30}$$

We have chosen the nonlinearity parameter, K, to lie in the interval $[0,1]$. Therefore each element of $C + D$ is guaranteed to be non-negative. This implies that $C + D$ is a non-negative irreducible matrix. According to the Frobenius-Perron theorem [Appendix A 1], the matrix $C + D$ has one eigenvalue λ which is greater than or equal to all other eigenvalues. Let $(C - D)^+$ be the matrix constructed by taking the modulus of each of the element in $C - D$. Its easy to see that each element of $(C + D)$ is greater than equal to the corresponding element of the matrix $(C - D)^+$. So the relation $(C + D) \geqslant (C - D)^+$ is valid. Then according to Wielandt's lemma [Appendix A 2], the modulus of any eigenvalue of $C - D$ is less than equal to the largest eigenvalue λ of $C + D$. So the largest eigenvalue of the Jacobian for the two-copy splay state is the

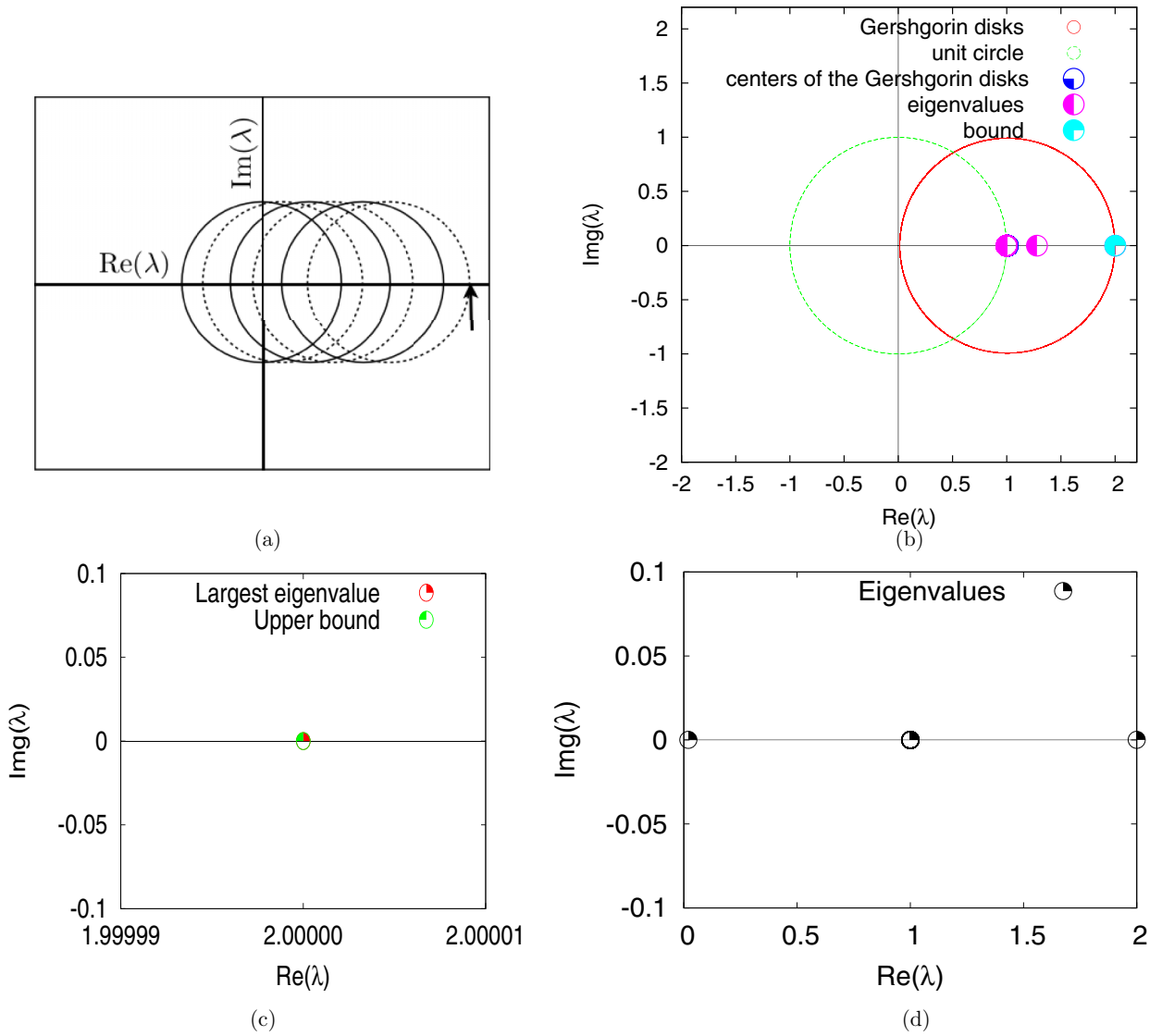

FIG. 4. (a) The schematic of the Gershgorin disks in the complex plane of the eigenvalues. The arrowhead points to the value of the upper bound. (b) The Gershgorin disks for the one-step matrix J^*_{2S} are shown. The parameters are $K = 10^{-10}$, $\Omega = \frac{2}{7}$, $\epsilon_1 = 0.01$, where we obtain a two-copy state as seen in Fig. 1(a). (c) The location of the upper bound and the largest eigenvalue. For these values of the parameters, the upper bound and the largest eigenvalue coincide to graphical accuracy. (d) The numerically calculated eigenvalues for a system with 150 lattice sites in each group.

largest eigenvalue in $C + D$. We calculate the upper bound of this largest eigenvalue and check whether the numerically calculated eigenvalues are within this limit. We use the Gershgorin's theorem (Appendix A 3) for this purpose.

Upper bound on the eigenvalues of the Jacobian

The bounds on the eigenvalues are obtained by constructing the Gershgorin disks, whose centers have values given by the diagonal elements of the matrix of interest and whose radii are given by the sum of the off-diagonal elements in the row or column. The diagonal elements of the matrix $C + D$ are real and nonnegative, which implies that the Gershgorin row region and the column region will consist of disks whose centers lie on the real axis. For the state with two copies of splay states the center (c_j) of the jth Gershgorin disk is $(1 + \frac{\epsilon_1+\epsilon_2}{N})[1 - K\cos(2\pi\theta_0 + \frac{2\pi j}{2N})]$. The radius of the jth disk in the Gershgorin row region r_j is

$$r_j = \frac{\epsilon_1+\epsilon_2}{N}\left\{\sum_{i=0}^{N-1}\left|1 - K\cos\left[2\pi\theta(0) + \frac{\pi i}{N}\right]\right| - \left|1 - K\cos\left[2\pi\theta(0) + \frac{\pi j}{N}\right]\right|\right\} \tag{31}$$

or

$$r_j = \frac{N-1}{N} - \frac{K}{N} \times \left\{\frac{\cos[2\pi\theta(0)]\left(1 - \cos\frac{\pi}{N}\right) - \sin[2\pi\theta(0)]\sin\left(\frac{\pi}{N}\right)}{1 - \cos\left(\frac{\pi}{N}\right)}\right\} + \frac{K}{N}\cos\left[2\pi\theta(0) + \frac{\pi j}{N}\right]. \tag{32}$$

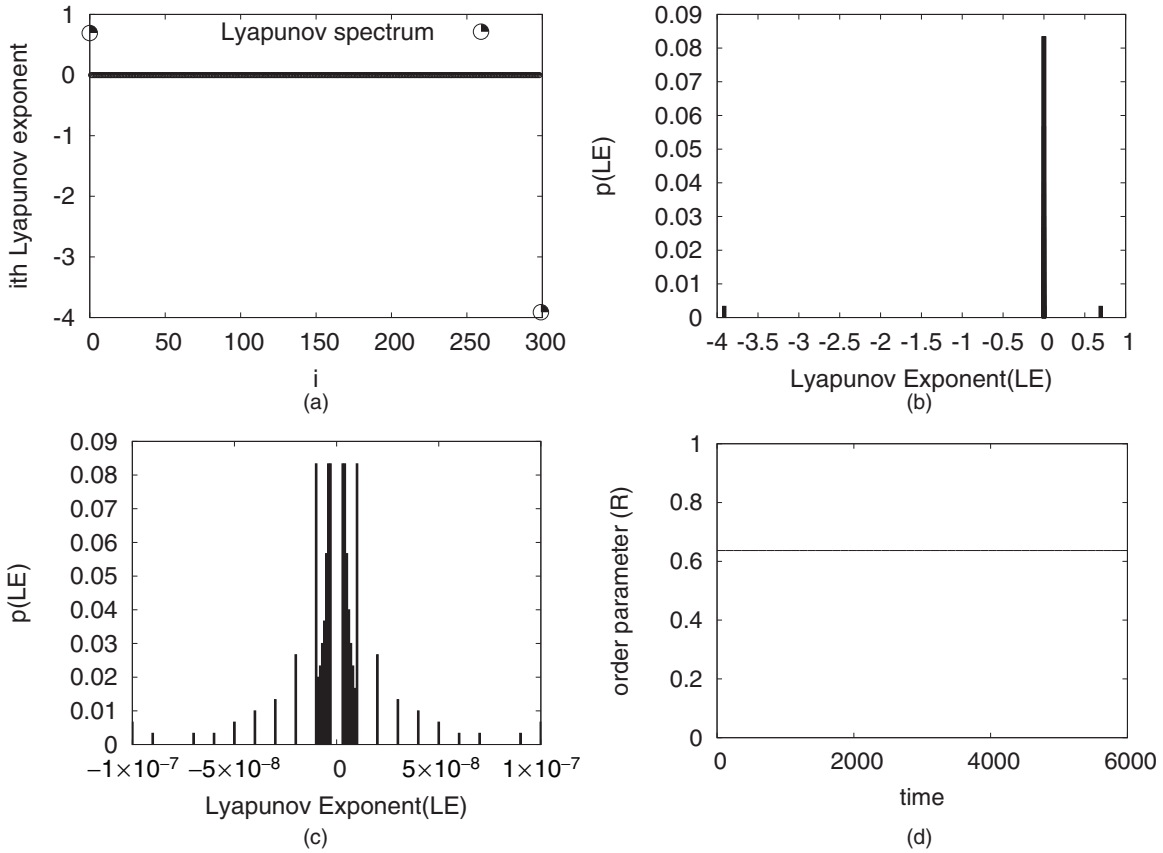

FIG. 5. The Lyapunov spectrum at $K = 10^{-10}$, $\Omega = 2/7$, $\epsilon_1 = 0.01$ for the two-copy splay states. The two circles denote the largest and the smallest Lyapunov exponent, and the smaller points are those which are very near to zero. (b) A histogram showing the distribution of Lyapunov exponents. (c) A magnified version of the distribution of the Lyapunov exponents near zero. (d) The variation of the order parameter with time for 6000 steps.

The radius of the ith disk in the column region is

$$s_i = \frac{N-1}{N}\left\{1 - K\cos\left[2\pi\theta(0) + \frac{\pi i}{N}\right]\right\}. \tag{33}$$

Since the centers of every disk in the Gershgorin row and column region lie on the real axis, the two bounds set by the Gershgorin row and column regions are given by the two largest numbers at which the discs from each of these sets intersect the real axis, i.e., $\max(c_j + r_j)$ and $\max(c_i + s_i)$. The required bound on the eigenvalues is the minimum of these two values. So the upper bound on the eigenvalues of Jacobian for the two-splay copies is

$$\min(\max(c_j + r_j), \max(c_i + s_i))$$

with $1 \leqslant j \leqslant N$ and $1 \leqslant i \leqslant N$. The Gershgorin disk and the bound on the eigenvalues obtained from them is plotted in Figs. 4(a) and 4(b). The largest eigenvalue obtained numerically by diagonalizing the matrix J_{2S}, is also shown, for the parameter values in Fig. 4(d). It is clear that the eigenvalue saturates the bound here.

If we have a state with exactly k copies of splay states throughout the system and each of them consists of $2N/k$ number of maps, then we can also calculate the upper bound on the eigenvalues of the Jacobian due that state (Appendix B 1). In that case the upper bound is given by

$$\min\Bigg(\max\Bigg\{2 - \frac{kK}{2N}\sum_{j=0}^{\frac{2N}{k}-1}\cos\left[2\pi\theta(0) + \frac{\pi j}{N}\right] - K\cos\left[2\pi\theta(0) + \frac{\pi j}{N}\right]\Bigg\}, \times \max\left\{2 - 2K\cos\left[2\pi\theta(0) + \frac{\pi i}{N}\right]\right\}\Bigg)$$

for $1 \leqslant i,\ j \leqslant \frac{2N}{k} - 1$. We can also calculate the upper bound on the eigenvalues if this k copy splay state has a temporal period Q (Appendix B 2). The form of the upper bound in this case is given by

$$\max\left[\max\left(\left(1 + \frac{1}{N}\right)\{1 - K\cos[2\pi\theta^j(i)] + R(A^j + B^j, i)\}\right)\right], \tag{34}$$

where A^j, B^j are block matrices which constitute the Jacobian for the step j and $R(A^j + B^j, i)$ is the sum of the elements of

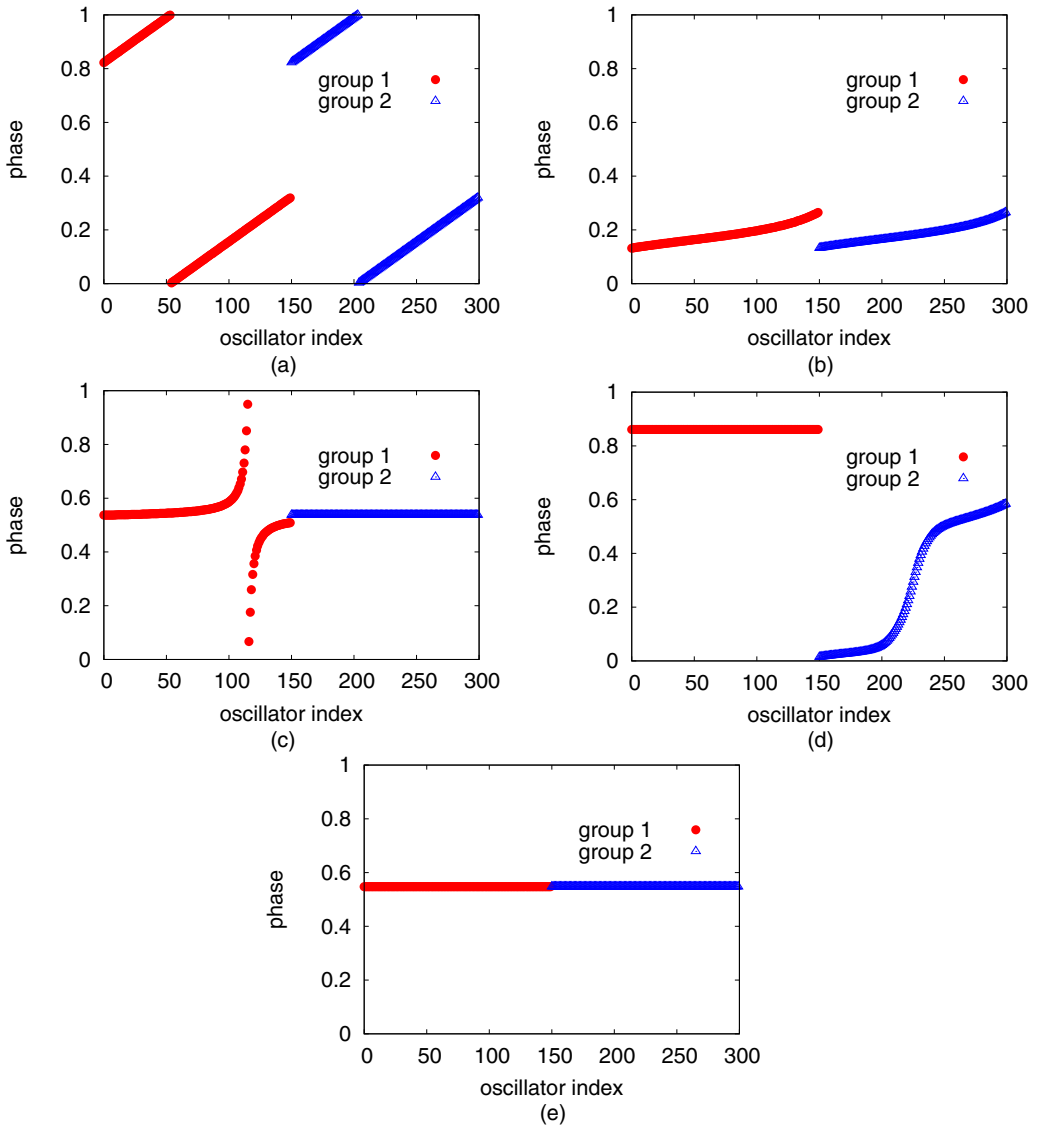

FIG. 6. (a) Given an initial condition where the all the maps constitute a spatial splay state [Fig. 2(a)] we obtain two copies of the splay state after evolution. The system, with 150 circle maps in each group, was iterated for 3 000 000 steps. Splay states were obtained at parameter values $K = 10^{-11}$, $\Omega = \frac{2}{7}$, $\epsilon_1 = 0.01$. (b) For the parameter values $K = 10^{-6}$, $\Omega = \frac{2}{7}$, $\epsilon_1 = 0.01$ the two groups still synchronize, but the size of the splay states decrease. (c) For the same values of Ω and ϵ_1 if we increase K to 10^{-4}, then the maps in group 2 synchronize completely [i.e., sites (150–300)], and in group 1, the phases of some maps are part of a splay-like state (roughly between sites 1 to 100 and 130 to 150) whereas the remaining maps show a jump (roughly between site 100 and 130) in their phases. (d) For $K = 10^{-2}$, $\Omega = \frac{2}{7}$, $\epsilon_1 = 0.01$ the behavior between group 2 maps and group 1 maps is interchanged. (e) Increasing K to 1 gives a global synchronized state.

the ith row of the matrix $A^j + B^j$ except only the diagonal element and $1 \leqslant j \leqslant Q, 0 \leqslant i \leqslant N-1$.

Except for the case with a temporal period Q, we note that the analysis here is for a single-step stability matrix. To consider the temporal behavior of the two-copy spatial splay state, we examine the Lyapunov exponent of the system. This is discussed in the next section.

IV. TEMPORAL BEHAVIOR AND BIFURCATIONS

A. Lyapunov exponents and order parameter for the two-copy spatial splay states

The numerically calculated largest eigenvalue of the one-step Jacobian [Fig. 4(d)] for the two-copy splay state turns out to exceed one. However, we also see that the splay states maintain their spatial structure upon further iterations. These suggest that this two-copy splay state may be temporally chaotic. To confirm this, we numerically calculated the largest Lyapunov exponent for 10^6 points on the trajectory, after discarding the initial 3×10^6 iterations and for the next 10^6 points on the trajectory using the Gram-Schmidt procedure at each step. Following this process, the largest Lyapunov exponent turns out to be 0.693, which indicates that the trajectory of the two-copy splay state is temporally chaotic. The sum of the Lyapunov exponents is negative, which implies that the system is dissipative. Figure 5(a) shows that almost all the Lyapunov exponents lie near zero. The probability distribution for the Lyapunov spectrum shows a peak around

zero [Fig. 5(b)]. To show that the phase distribution of the maps in this two-copy chaotic splay states is stable, we calculate, at each time step, the order parameter $r = |\langle \exp(i2\pi\theta)\rangle|$ [31] where the average is taken over all the maps with same dynamics. We calculate this quantity by taking the average over the whole system since we have two splay copies and they also synchronize. We calculate this quantity for 10^6 time steps after neglecting the initial transient steps. Figure 5(d) clearly shows that phase distribution of maps for the two-copy splay states is stable.

We note that the two-copy spatial splay state undergoes bifurcations to other kinds of states with increase in the nonlinearity parameter. We discuss these in the next subsection.

B. Bifurcation

We note that the two-copy spatial splay state resulting from a single-splay initial condition bifurcates to other kinds of states if the nonlinearity parameter is increased. The splay state bifurcates to other synchronized states and mixed states. We list the states that can be observed if we increase K. For each case the initial condition was the single spatial splay state as in Fig. 2(a). Four possible states were seen after the bifurcation.

(1) The two-copy pure spatial splay states are observed [Fig. 6(a)] when the nonlinearity parameter K is below 10^{-7}. They appear in the range $0 < K < 10^{-7}$. (2) In this snapshot, the phase of the ith map and $(i + 150)$th map are equal, and they maintain this equality as they evolve in time. The difference between the consecutive maps in each group increases very slowly with i resulting in a two-copy splay-like structure. This configuration appears approximately in the range $10^{-6} < K < 10^{-5}$. (3) When K is around 10^{-4} we obtain another kind of mixed state. Here we see that phases of the maps in one group remain spatially synchronized (sites 151–300) and in the other group, the phases of some of the maps show a splay-like diagonal structure (sites 1–100, 130–150) while the remaining maps show phase jumps (100–130) [Fig. 6(c)]. (4) If we increase K even higher, then near $K \approx 10^{-2}$ the mixed state remains the same, but the behavior of the two groups is interchanged [Fig. 6(d)]. Now all the maps in group 1 are spatially synchronized, and in group 2, maps at sites roughly between 200 and 250 show a phase jump and sites 151 to 200 and 250 to 300 show a splay-like diagonal structure. These splay-chimera configurations appear approximately in the range $10^{-4} < K < 0.05$. (5) For K above 0.05, all the maps are spatially phase synchronized [Fig. 6(e)]. We calculate the global order parameter $R' = \sum_{i=1}^{2N} e^{i2\pi}/2N$ for the entire lattice for the entire range of range of K value for which the dynamical states in Fig. 6 appear and plot this in Fig. 7(a). We observe that in the regime of the two-copy spatial splay states $0 < K < 10^{-7}$ and two-copy splay-like states $10^{-6} < K < 10^{-5}$, the time variation of the order parameter R' indicates that both the structures are stable with respect to the variation of K. Between these two regimes the spatial splay states start to bifurcate to splay-like states as in Fig. 6(b) with slopes decreasing with the variation of K. We thus see that R' increases between $K = 10^{-7}$ and $K = 10^{-6}$. We further observe that the global order parameter R' fluctuates in the range $10^{-4} < K < 0.05$, which indicates a variation within

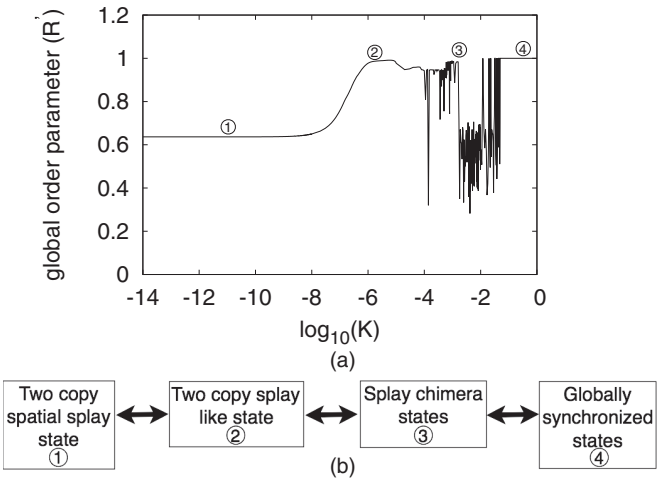

FIG. 7. (a) The order parameter is calculated for K taking values between zero to one. For each value of K, Eq. (2) is iterated for 3×10^6 times using the single splay initial condition after which the order parameter for the whole system is calculated. (b) The bifurcation route which was realized using $\epsilon_1 = 0.01$ and $\Omega = \frac{2}{7}$ and varying K from 0 to 1.

the splay-chimera structures. We can also observe the onset of global synchronization in Fig. 7(a) when R' goes to one near $K \approx 0.05$. A schematic of this entire bifurcation route is shown in Fig. 7(b).

For constant Ω and ϵ_1 we plot the bifurcation diagram for a typical site of the system by varying K from 0 to 1 [Figs. 8(a)–8(e)]. We see that the phases of each site for the splay states, live inside a thin chaotic band [Fig. 8(a)]. The phase space available to a single site increases in size when the system shows two synchronizing mixed states [Figs. 8(b) and 8(c)]. In the cases of single mixed states we observe that the available phase space spans from 0 to 1 for a single site [Fig. 8(d)]. This scenario remains the same for the globally synchronized case also [Fig. 8(e)]. Figure 8(f) shows that the largest Lyapunov exponent is positive up to $K = 1$ implying that all the trajectories for the states in Figs. 5(a)–5(e) are temporally chaotic.

C. Chimera splay state

As mentioned above, the spatial splay states bifurcate to mixed splay states or chimera splay states with increase in the value of the nonlinearlity parameter K. We obtain the mixed splay states when the value of K is roughly between 10^{-5} and 10^{-2}. For values of K near 10^{-4} we observe that the mixed state consists of an entire group where all the maps are phase synchronized, and in the other group, some maps are organized in a splay-like diagonal structure and the rest of the maps have phase jumps [Figs. 6(c) and 6(d)]. We calculate the complex order parameter $r(t) = |\langle \exp(i2\pi\theta)\rangle|$ for the desynchronized group, which contains the mixed states of splay-like diagonal structure and the state with phase jumps. Figure 9(a) shows that this order parameter is stable, implying that the structure remains stable with time. For values of K around 10^{-2} we see that the behavior of the maps in the two groups are interchanged. The order parameter calculated

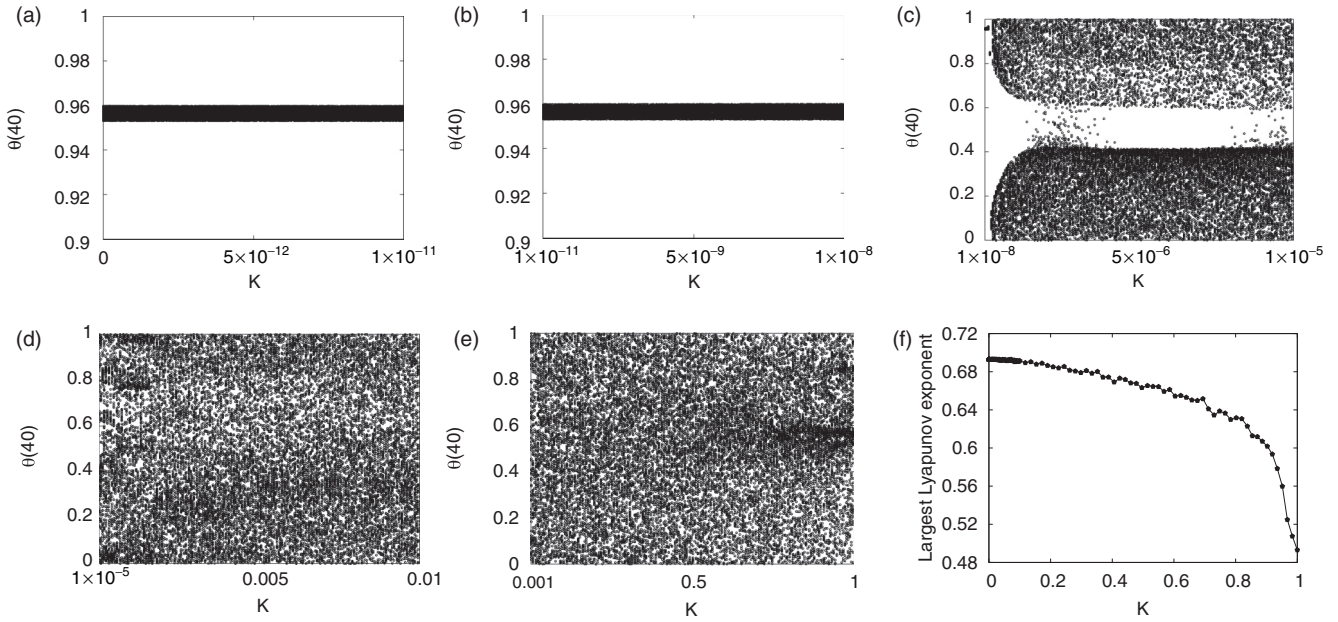

FIG. 8. (a–e) Bifurcation diagram for the map at site 40 in group 1 for different ranges of the values of K. For each value of K the initial 3×10^6 time steps are neglected and the next 5000 values are taken. (f) The variation of the largest Lyapunov exponent for K between 0 and 1.

for the desynchronized subgroup in that case indicates its aperiodic nature [Fig. 9(b)]. On the other hand, the calculation of the order parameter for the synchronized groups (group 2 for $K = 10^{-4}$, and group 1 for $K = 10^{-2}$) shows that they remain synchronized with time.

We also calculate the largest Lyapunov exponent for the above two cases. For both of these we get a positive largest Lyapunov exponent. For both the parameter values $K = 10^{-4}$, 10^{-2} the largest Lyapunov exponent is positive and takes the value $\lambda_{\text{largest}} = 0.693$ and the smallest Lyapunov exponent is $\lambda_{\text{smallest}} = -3.91$ (See Fig. 10).

D. Response to perturbation

In this section we study the response of two copy splay states to perturbations of very low strength. Let $\Theta_n\{\theta_n^1(1), \theta_n^1(2), \ldots, \theta_n^1(N), \theta_n^2(1), \theta_n^2(2), \ldots, \theta_n^2(N)\}$ be the original phases at time step n. We choose the perturbation of the form $\kappa\zeta_\kappa$, where κ is strength of perturbation and ζ_κ is a random number between 0 and 1. First we iterate Eq. (2) using the system-wide single splay state as the initial condition [Fig. 2(a)], in the parameter region where two copy splay states are observed as the final state. At a given time step ($n = 10^6$) we introduce the perturbation so that the evolution equation has the form

$$\theta_{n+1}^{\sigma}(i) = \theta_n^{\sigma}(i) + \Omega - \frac{K}{2\pi}\sin\left[2\pi\theta_n^{\sigma}(i)\right] + \sum_{\sigma'=1}^{2}\frac{\epsilon_{\sigma\sigma'}}{N_{\sigma'}}\left\{\sum_{j=1}^{N_{\sigma'}}\left(\theta_n^{\sigma'} + \Omega - \frac{K}{2\pi}\sin\left[2\pi\theta_n^{\sigma'}\right]\right)\right\} + \kappa\zeta_\kappa \mod 1. \tag{35}$$

From the next step we turn off the perturbation and follow the two trajectories, (1)$\Theta_n\{\theta_n^1(1),\theta_n^1(2),\ldots,\theta_n^1(N), \theta_n^2(1), \theta_n^2(2),\ldots,\theta_n^2(N)\}$ corresponding to the unperturbed splay state and (2) $\Theta'_n\{\theta_n'^1(1), \theta_n'^1(2),\ldots,\theta_n'^1(N), \theta_n'^2(1), \theta_n'^2(2),\ldots,\theta_n'^2(N)\}$ corresponding to the perturbed trajectory. We calculate the Euclidean distance between these two trajectories, i.e.,

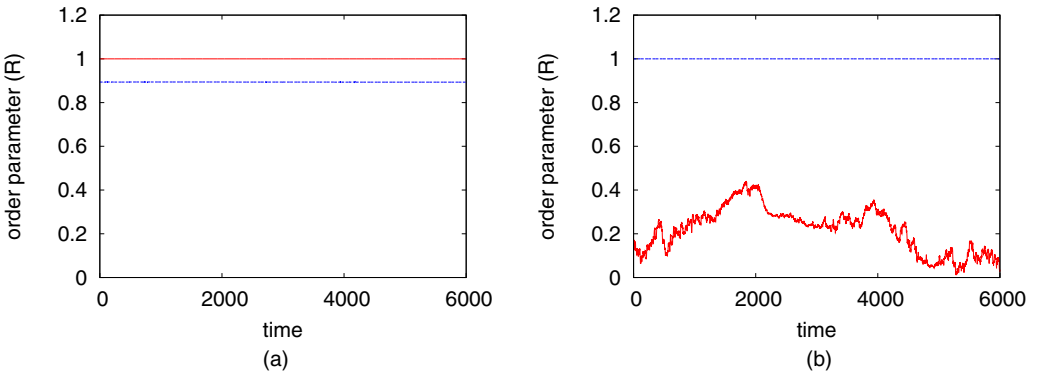

FIG. 9. (a) Order parameter for group 1 (blue) and group 2 (red) at (a) $K = 10^{-4}$ and group 2 at (b) $K = 10^{-2}$ with $\epsilon_1 = 0.01$ and $\Omega = 2/7$.

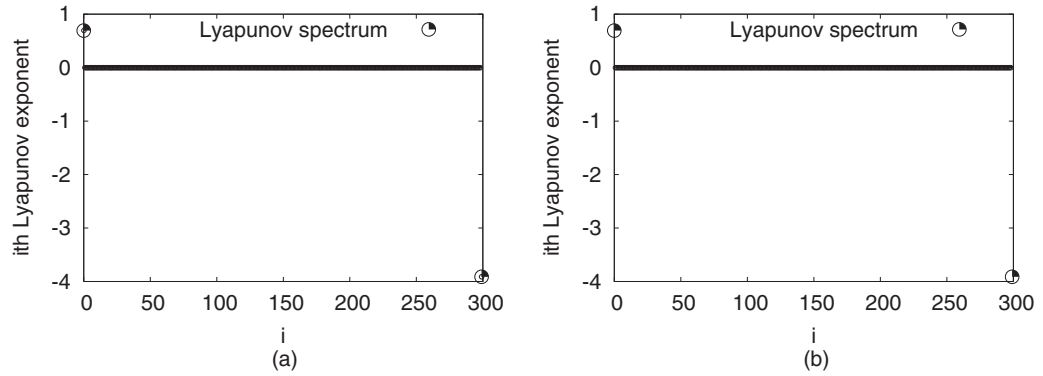

FIG. 10. Lyapunov spectrum of system 2 at parameters (a) $K = 10^{-4}$, (b) $K = 10^{-2}$ with $\epsilon_1 = 0.01$ and $\Omega = 2/7$.

$\sqrt{\sum_{i=1}^{i=2N}[\theta_n(i) - \theta'_n(i)]^2/2N}$, at each time step. Using a small value of κ ($\kappa = 10^{-7}$) we calculate the Euclidean distance for the next two million steps. Figure 11(a) shows that the perturbed trajectory evolves in the neighborhood of the original trajectory in an aperiodic fashion. We also observe that the variation of the Euclidean distance with time shows (1) laminar regions where the variation in the distance between the trajectories at successive time steps is less that 10^{-5} and (2) burst regions where the variation in the distance between successive time steps exceeds this threshold. Let l and l' denote the lengths of these laminar and burst regions. The distribution of the probabilities for the occurrence of laminar regions of length l follows stretched exponential

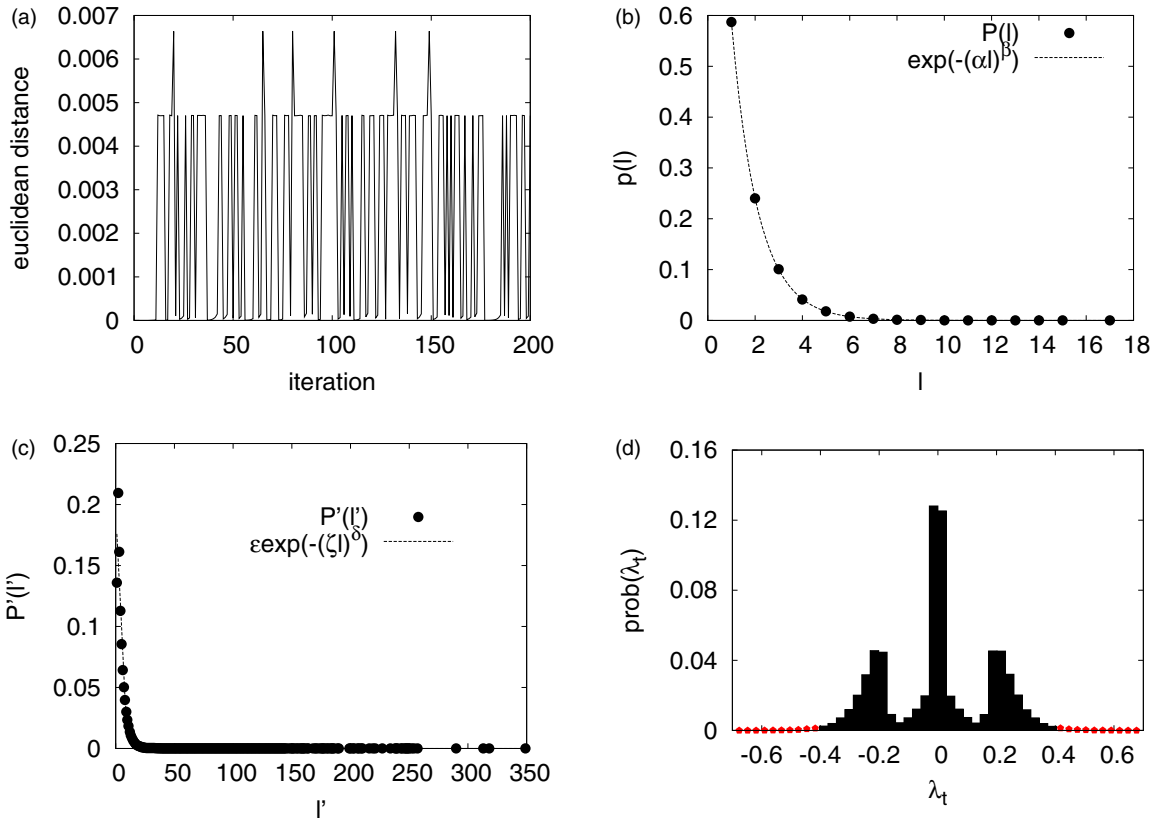

FIG. 11. (a) The plot of the Euclidean distance vs the number of iterations for $\kappa = 10^{-5}$, $K = 10^{-10}$, $\Omega = 2/7$, $\epsilon_1 = 0.01$. The initial condition was a single-splay state through out the system. The time steps on the x axis are from the time step at which the perturbation was given. (b) The distribution of the probability of occurrence of laminar regions of length l vs the length of the laminar regions. The function $\exp(-\alpha l^{\beta})$ was fitted to this distribution with $\alpha = 0.934 \pm 0.007$, $\beta = 0.966 \pm 0.005$. (c) The plot of the probability of occurrence of bursts region of length l' vs the length l' of the burst regions. The function $\exp[(-\zeta l')^{\delta}]$ is fitted to this. This gives $\zeta = 0.154 \pm 0.007$, $\delta = 1.944 \pm 0.255$. (d) The FTLEs are calculated using time intervals of 21 steps for a total of 3×10^6 time steps. The histogram is plotted using 50 bins between $[-0.72, 0.72]$. The largest FTLE is 0.691. The red dots denote the FTLEs whose probability of occurrence is near 10^{-6}. The values $\kappa = 10^{-7}$, $\tau = 10^{-5}$, $K = 10^{-10}$, $\Omega = 2/7$, $\epsilon_1 = 0.01$ were used for the above plots.

behavior given by

$$P(l) = \exp[-(\alpha l)^{\beta}], \tag{36}$$

whereas the distribution of probabilities for the existence of burst regions of length l' follows the behavior

$$P'(l') = \exp[-(\zeta l')^{\delta}]. \tag{37}$$

The numerical values of the constants $\alpha, \beta, \zeta, \delta$ can be found in the captions of Figs. 11(b) and 11(c). These numerical values depends on the strength of perturbation, i.e., κ to the original trajectory, i.e., these constants depend on how far the perturbed trajectory is from the original trajectory. However, the functional forms of $P(l), P(l')$, i.e., Eqs. (36) and (37) are seen to be the independent of κ and are similar to the behavior seen in random walks in the presence of traps.

The probability distribution of the finite time Lyapunov exponents [Fig. 11(d)], calculated from the data of the time series in Fig. 11, shows that most of the FTLEs lie near zero, while the largest FTLE is 0.69, which is close to the value of the largest LE calculated by taking a long time average in Sec. IV A. The perturbed and the original trajectory, while moving through the different parts of the phase space, come closer when there are locally dominant contracting directions and move apart from each other when there are locally dominant expanding directions. The laminar regions are obtained when the trajectories maintain a constant distance, corresponding to regimes where the neutral directions are dominant. The perturbation strength is sufficiently low [13] so that no hopping between multiple attractors occurs. The regions where the dominant local behavior is contracting function as traps, leading to the stretched exponential behavior seen in Figs. 11(b) and 11(c).

V. CONCLUSION

In this paper we consider a globally coupled system of two groups of sine circle maps, with different values of intragroup and intergroup coupling. This system shows the existence of a variety of solutions. Here we concentrate on the analysis of spatial splay states, viz., states where the phase difference between maps at successive sites is a constant. Such states and their multiple copies are obtained when the system is evolved with an initial condition which is a spatial splay state, and for a regime where the nonlinearity constant K takes very small values, i.e., the system is very close to a system of coupled shift maps. We carry out the stability analysis of the system and use the Gershgorin theorem to obtain analytic bounds on the eigenvalues. The numerical analysis of the system at certain parameter values shows that the largest eigenvalue nearly saturates the analytic bound. Such states are found to be temporally chaotic. Bifurcations from the spatial splay states are also studied and show that the resulting states can be chimera splay states, splay states with kinks, and globally synchronized states. Finally, we examine the stability of the spatial splay states to perturbation and observe the existence of stretched exponential behavior in the distributions of laminar lengths in the time series of the Euclidean distance between states. We note that the possibility of hysteresis and multiattractor solutions exists in this system. We hope to explore this in future work.

We note that splay states as defined in Refs. [6–10] have been earlier observed in Josephson junction arrays, coupled oscillator systems, and chemical reactions. We hope to examine whether the spatial splay states and some of the features observed here can be seen in these systems. Finally, the system studied represents a discrete realization of a coupled oscillator system. We therefore hope that some of the features observed over here can be seen in experimentally realizable systems as well.

ACKNOWLEDGMENTS

One of the authors (J.S.) acknowledges the support of the University Grants Commission, India, in the form of a research fellowship. The other author (N.G.) thanks CSIR, India for partial support under the Grant No. 03(1264)13/EMR-II, and IIT Madras for support under the exploratory research proposal ERP1314024RESFNEEL.

APPENDIX A: THEOREMS

1. Frobenius-Perron theorem

Any non-negative irreducible matrix A always has a positive eigenvalue λ, which is a simple root of its characteristic polynomial and the moduli of all the other eigenvalues are less than or equal to λ.

2. Wielandt's lemma

Let A be a irreducible square matrix and B is a square matrix of order n. Let B^+ be the matrix constructed by taking the modulus of elements of B, then if $A \geqslant B^+$, then the modulus of any eigenvalue of B^+ is less than the largest eigenvalue of A.

3. Gershgorin's theorem

Each eigenvalue of a complex matrix A $\{a_{ij}\}$ of order N lies in at least in one of the disks

$$\mathscr{D}_i(A) = \{z : |z - a_{ii}| \leqslant R_i\} \tag{A1}$$

for $1 \leqslant i \leqslant N$ on the complex plane and $R_i = \sum_{\substack{j=1 \\ j\neq i}}^{n} a_{ij}$. In other words the N eigenvalues of the complex plane are contained in a region in the complex plane determined by

$$\mathscr{D}(A) = \bigcup_{i=1}^{n} \mathscr{D}_i(A). \tag{A2}$$

Similarly from $A^T\{a_{ji}\}$ the Gershgorin column region can be found, which is

$$\mathscr{D}'(A) = \bigcup_{j=1}^{n} \mathscr{D}'_j(A) \tag{A3}$$

with $\mathscr{D}'_j(A) = \{z : |z - a_{jj}| \leqslant S_j\}$ and $S_j = \sum_{\substack{i=1 \\ i\neq j}}^{n} a_{ji}$. So all the eigenvalues lie in the region $\mathscr{D}(A) \cap \mathscr{D}'(A)$.

APPENDIX B: SPATIALLY AND TEMPORALLY PERIODIC SPLAY STATES

1. Splay states with spatial period k

The upper bound on the eigenvalues of the Jacobian for k copies of splay state can also be found out. We assume that there are exactly $\frac{k}{2}$ copies of splay state in each group so that there will be exactly $\frac{2N}{k} - 1$ number. So we can

still reduce the Jacobian in to a block circulant matrix. The inequality $(A+B) \geqslant |A-B|^{+}$ is still valid in this case, and the matrix $A+B$ is non-negative and irreducible. So again according to Frobenious-Perron theorem and Wielandt's lemma, the largest eigenvalue of $A+B$ greater than equal to any eigenvalue of the matrix $A-B$. In the Gershgorin region due to the matrix $A+B$, there will be $\frac{k}{2}$ discs, both in the Gershgorin column region and row region. The distance of the center (C_j^k) of the jth Gershgorin disk from the origin either in the column or the row region for the matrix $A+B$ is $(1+\frac{\epsilon_1+\epsilon_2}{N})(1-K\cos[2\pi\theta(0)+\frac{\pi j}{N}])$. The radius r_j^k of the jth disk in the row region is

$$r_j^k = \frac{k(\epsilon_1+\epsilon_2)}{2N}\left\{\sum_{j=0}^{\frac{2N}{k}-1}\left|1-K\cos\left[2\pi\theta(0)+\frac{\pi j}{N}\right]\right| - \left|1-K\cos\left[2\pi\theta(0)+\frac{\pi j}{N}\right]\right|\right\}. \tag{B1}$$

The radius s_i^k of the ith disk in the Gershgorin column region i is given by

$$s_i^k = \frac{(N-1)(\epsilon_1+\epsilon_2)}{N}\left\{1-K\cos\left[2\pi\theta(0)+\frac{\pi i}{N}\right]\right\}. \tag{B2}$$

The diagonal elements of the matrix $A+B$ are real so as it was for the two copies of splay states the bounds on the eigenvalues of the Jacobian set by the Gershgorin row and column regions of $A+B$ for k-splay copies are $\max(c_j^k+r_j^k)$ and $\max(c_i^k+s_i^k)$. So the upper bound is

$$\min\left(\max\left\{2-\frac{kK}{2N}\sum_{j=0}^{\frac{2N}{k}-1}\cos\left[2\pi\theta(0)+\frac{\pi j}{N}\right]-K\cos\left[2\pi\theta(0)+\frac{\pi j}{N}\right]\right\},\ \max\left\{2-2K\cos\left[2\pi\theta(0)+\frac{\pi i}{N}\right]\right\}\right)$$

for $1 \leqslant i,\ j \leqslant \frac{2N}{k}-1$.

2. Splay states with spatial period k and temporal period Q

The upper bound on the eigenvalues of the Jacobian for k-splay copies with temporal period Q can be calculated via an extension version of the Gershgorin theorem [20] provided that group 1 and group 2 are always exact copies of each other. In terms of the phases of the maps such solution would be of the form $\{\theta^1(0),\theta^1(1),\ldots,\theta^1(\frac{2N}{k}-1),\theta^1(0),\ \theta^1(1),\ldots,\theta^1(\frac{2N}{k}-1),\ldots,\theta^1(0),\ \theta^1(1),\ldots,\theta^1(\frac{2N}{k}-1)\}$, $\{\theta^2(0),\theta^2(1),\ldots,\theta^2(\frac{2N}{k}-1),\theta^2(0),\theta^2(1),\ldots,\theta^2(\frac{2N}{k}-1),\ldots,\theta^2(0),\theta^2(1),\ldots,\theta^2(\frac{2N}{k}-1)\},\ldots,\{\theta^Q(0),\theta^Q(1),\ldots,\theta^Q(\frac{2N}{k}-1),\theta^Q(0),\theta^Q(1),\ldots,\theta^Q(\frac{2N}{k}-1),\ldots,\theta^Q(0),\theta^Q(1),\ldots,\theta^Q(\frac{2N}{k}-1)\}$. The Jacobian corresponding to this state is

$$J = \begin{pmatrix} A^1 & B^1 \\ B^1 & A^1 \end{pmatrix}\begin{pmatrix} A^2 & B^2 \\ B^2 & A^2 \end{pmatrix}\cdots\begin{pmatrix} A^Q & B^Q \\ B^Q & A^Q \end{pmatrix} \tag{B3}$$

with

$$A^i = \begin{bmatrix} (1+\frac{\epsilon_1}{N})\{1-K\cos[2\pi\theta^i(0)]\} & \cdots & \frac{\epsilon_1}{N}\{1-K\cos[2\pi\theta^i(\frac{2N}{k}-1)]\} & \cdots & \frac{\epsilon_1}{N}\{1-K\cos[2\pi\theta^i(\frac{2N}{k}-1)]\} \\ \frac{\epsilon_1}{N}\{1-K\cos[2\pi\theta^i(0)]\} & \cdots & \frac{\epsilon_1}{N}\{1-K\cos[2\pi\theta^i(\frac{2N}{k}-1)]\} & \cdots & \frac{\epsilon_1}{N}\{1-K\cos[2\pi\theta^i(\frac{2N}{k}-1)]\} \\ \cdots & \cdots & \cdots & \cdots & \cdots \\ \frac{\epsilon_1}{N}\{1-K\cos[2\pi\theta^i(0)]\} & \cdots & \frac{\epsilon_1}{N}\{1-K\cos[2\pi\theta^i(\frac{2N}{k}-1)]\} & \cdots & (1+\frac{\epsilon_1}{N})\{1-K\cos[2\pi\theta^i(\frac{2N}{k}-1)]\} \end{bmatrix} \tag{B4}$$

and

$$B^i = \begin{bmatrix} \frac{\epsilon_2}{N}\{1-K\cos[2\pi\theta^i(0)]\} & \cdots & \frac{\epsilon_2}{N}\{1-K\cos[2\pi\theta^i(\frac{2N}{k}-1)]\} & \cdots & \frac{\epsilon_2}{N}\{1-K\cos[2\pi\theta^i(\frac{2N}{k}-1)]\} \\ \frac{\epsilon_2}{N}\{1-K\cos[2\pi\theta^i(0)]\} & \cdots & \frac{\epsilon_2}{N}\{1-K\cos[2\pi\theta^i(\frac{2N}{k}-1)]\} & \cdots & \frac{\epsilon_2}{N}\{1-K\cos[2\pi\theta^i(\frac{2N}{k}-1)]\} \\ \cdots & \cdots & \cdots & \cdots & \cdots \\ \frac{\epsilon_2}{N}\{1-K\cos[2\pi\theta^i(0)]\} & \cdots & \frac{\epsilon_2}{N}\{1-K\cos[2\pi\theta^i(\frac{2N}{k}-1)]\} & \cdots & \frac{\epsilon_2}{N}\{1-K\cos[2\pi\theta^i(\frac{2N}{k}-1)]\} \end{bmatrix}. \tag{B5}$$

Each of the matrices in the Jacobian can be block diagonalized by $\mathbf{P}$ [Eq. (19)] so that the Jacobian itself turns into a block diagonalized form,

$$\mathbf{P}^{-1}J\mathbf{P} = \begin{pmatrix} A^1+B^1 & 0 \\ 0 & A^1-B^1 \end{pmatrix}\begin{pmatrix} A^2+B^2 & 0 \\ 0 & A^2-B^2 \end{pmatrix}\cdots\begin{pmatrix} A^Q+B^Q & 0 \\ 0 & A^Q-B^Q \end{pmatrix} \tag{B6a}$$

$$= \begin{pmatrix} (A^1+B^1)(A^2+B^2)\cdots(A^Q+B^Q) & 0 \\ 0 & (A^1-B^1)(A^2-B^2)\cdots(A^Q-B^Q) \end{pmatrix}, \tag{B6b}$$

where

$$A^i + B^i = \begin{bmatrix} \left(1+\frac{\epsilon_1+\epsilon_2}{N}\right)\{1-K\cos[2\pi\theta^i(0)]\} & \cdots & \frac{\epsilon_1+\epsilon_2}{N}\left\{1-K\cos\left[2\pi\theta^i\left(\frac{2N}{k}-1\right)\right]\right\} & \cdots & \frac{\epsilon_1+\epsilon_2}{N}\left\{1-K\cos\left[2\pi\theta^i\left(\frac{2N}{k}-1\right)\right]\right\} \\ \frac{\epsilon_1+\epsilon_2}{N}\{1-K\cos[2\pi\theta^i(0)]\} & \cdots & \frac{\epsilon_1+\epsilon_2}{N}\left\{1-K\cos\left[2\pi\theta^i\left(\frac{2N}{k}-1\right)\right]\right\} & \cdots & \frac{\epsilon_1+\epsilon_2}{N}\left\{1-K\cos\left[2\pi\theta^i\left(\frac{2N}{k}-1\right)\right]\right\} \\ \cdots & \cdots & \cdots & \cdots & \cdots \\ \frac{\epsilon_1+\epsilon_2}{N}\{1-K\cos[2\pi\theta^i(0)]\} & \cdots & \frac{\epsilon_1+\epsilon_2}{N}\left\{1-K\cos\left[2\pi\theta^i\left(\frac{2N}{k}-1\right)\right]\right\} & \cdots & \left(1+\frac{\epsilon_1+\epsilon_2}{N}\right)\left\{1-K\cos\left[2\pi\theta^i\left(\frac{2N}{k}-1\right)\right]\right\} \end{bmatrix} \tag{B7}$$

and

$$A^i - B^i = \begin{bmatrix} \left(1+\frac{\epsilon_1-\epsilon_2}{N}\right)\{1-K\cos[2\pi\theta^i(0)]\} & \cdots & \frac{\epsilon_1-\epsilon_2}{N}\left\{1-K\cos\left[2\pi\theta^i\left(\frac{2N}{k}-1\right)\right]\right\} & \cdots & \frac{\epsilon_1-\epsilon_2}{N}\left\{1-K\cos\left[2\pi\theta^i\left(\frac{2N}{k}-1\right)\right]\right\} \\ \frac{\epsilon_1-\epsilon_2}{N}\{1-K\cos[2\pi\theta^i(0)]\} & \cdots & \frac{\epsilon_1-\epsilon_2}{N}\left\{1-K\cos\left[2\pi\theta^i\left(\frac{2N}{k}-1\right)\right]\right\} & \cdots & \frac{\epsilon_1-\epsilon_2}{N}\left\{1-K\cos\left[2\pi\theta^i\left(\frac{2N}{k}-1\right)\right]\right\} \\ \cdots & \cdots & \cdots & \cdots & \cdots \\ \frac{\epsilon_1-\epsilon_2}{N}\{1-K\cos[2\pi\theta^i(0)]\} & \cdots & \frac{\epsilon_1-\epsilon_2}{N}\left\{1-K\cos\left[2\pi\theta^i\left(\frac{2N}{k}-1\right)\right]\right\} & \cdots & \left(1+\frac{\epsilon_1-\epsilon_2}{N}\right)\left\{1-K\cos\left[2\pi\theta^i\left(\frac{2N}{k}-1\right)\right]\right\} \end{bmatrix}. \tag{B8}$$

Since each of the matrices $A^1+B^1, A^2+B^2, \ldots, A^Q+B^Q$ are nonnegative and irreducible so $(A^1+B^1)(A^2+B^2)\cdots(A^Q+B^Q)$ will also be nonnegative and irreducible. Let $[(A^1-B^1)(A^2-B^2)\cdots(A^Q-B^Q)]^+$ be the matrix obtained by taking the modulus of each element in $(A^1-B^1)(A^2-B^2)\cdots(A^Q-B^Q)$ then clearly

$$(A^1+B^1)(A^2+B^2)\cdots(A^Q+B^Q) \geqslant [(A^1-B^1)(A^2-B^2)\cdots(A^Q-B^Q)]^+. \tag{B9}$$

So according to Frobenious-Perron theorem and Wielandt's lemma, the largest eigenvalue of $(A^1+B^1)(A^2+B^2)\cdots(A^Q+B^Q)$ is always greater than equal to the eigenvalues of $(A^1-B^1)(A^2-B^2)\cdots(A^Q-B^Q)$. So the upper bound on the matrix $(A^1+B^1)(A^2+B^2)\cdots(A^Q+B^Q)$ is the upper bound on the eigenvalues of Jacobian of the system. Using the Gershgorin theorem for the product of nonsingular matrices [30] we find that it is

$$\max\left[\max\left(\left(1+\frac{1}{N}\right)\{1-K\cos[2\pi\theta^j(i)]+R(A^j+B^j,i)\}\right)\right], \tag{B10}$$

where $R(A^j+B^j,i)$ is the sum of the elements of the ith row of the matrix A^j+B^j except only the diagonal element and $1 \leqslant j \leqslant Q, 0 \leqslant i \leqslant N-1$.

[1] K. Kaneko, Physica D **68**, 299 (1993).
[2] K. Kaneko, Physica D **37**, 60 (1989).
[3] C. R. Nayak and N. Gupte, AIP Conf. Proc. **1339**, 172 (2011).
[4] S. Nkomo, M. R. Tinsley, and K. Showalter, Phys. Rev. Lett. **110**, 244102 (2013).
[5] A. M. Hagerstrom, T. E. Murphy, R. Roy, P. Hövel, I. Omelchenko, and E. Scholl, Nature Phys. **8**, 658 (2012).
[6] K. Y. Tsang, R. E. Mirollo, S. H. Strogatz, and K. Wiesenfeld, Physica D **48**, 102 (1991).
[7] K. Wiesenfeld and J. W. Swift, Phys. Rev. E **51**, 1020 (1995).
[8] S. Nichols and K. Wiesenfeld, Phys. Rev. A **45**, 8430 (1992).
[9] S. Nichols and K. Wiesenfeld, Phys. Rev. E **50**, 205 (1994).
[10] S. H. Strogatz and R. E. Mirollo, Phys. Rev. E **47**, 220 (1993).
[11] M. Calamai, A. Politi, and A. Torcini, Phys. Rev. E **80**, 036209 (2009).
[12] A. A. Selivanov, J. Lehnert, T. Dahms, P. Hövel, A. L. Fradkov, and E. Schöll, Phys. Rev. E **85**, 016201 (2012).
[13] K. Wiesenfeld and P. Hadley, Phys. Rev. Lett. **62**, 1335 (1989).
[14] K. Otsuka, Phys. Rev. Lett. **67**, 1090 (1991).
[15] D. A. Paley, N. E. Leonard, and R. Sepulchre, Oscillator models and collective motion: Splay state stabilization of self-propelled particles, in *Proceedings of the 44th IEEE Conference on Decision and Control, and European Control Conference 2005, Seville, Spain, December 12–15, 2005* (IEEE, Piscataway NJ, 2005).
[16] Y. N. Kyrychko, K. B. Blyuss, and E. Scholl, Chaos **24**, 043117 (2014).
[17] A. Nordenfelt, Chaos **25**, 113110 (2015).
[18] Y. Kuramoto and D. Battogtokh, Nonlinear Phenomena in Complex Systems **5**, 380 (2002).
[19] D. M. Abrams and S. H. Strogatz, Phys. Rev. Lett. **93**, 174102 (2004).
[20] G. C. Sethia, A. Sen, and F. M. Atay, Phys. Rev. Lett. **100**, 144102 (2008).
[21] J. N. Blakely, B. R. Reed, N. J. Corron, M. T. Stahl, and K. Myneni, Proc. SPIE 7669, Radar Sensor Technology XIV, 76690Q (April 23, 2010); doi:10.1117/12.850153.
[22] N. F. Rulkov, L. Tsimring, M. L. Larsen, and M. Gabbay, Phys. Rev. E **74**, 056205 (2006).
[23] G. R. Pradhan, N. Chatterjee, and N. Gupte, Phys. Rev. E **65**, 046227 (2002).
[24] M. H. Jensen, P. Bak, and T. Bohr, Phys. Rev. Lett. **50**, 1637 (1983).
[25] E. Ott, *Chaos in Dynamical Systems* (Cambridge University Press, Cambridge, 1993).

[26] J. Stavans, F. Heslot, and A. Libchaber, Phys. Rev. Lett. **55**, 596 (1985).
[27] L. Glass and M. C. Mackey, *From Clocks to Chaos: The Rhythms of Life* (Princeton University Press, Princeton, 1988).
[28] P. J. Davis, *Circulant Matrices* (Wiley, New York, 1979).
[29] N. Chatterjee and N. Gupte, Phys. Rev. E **63**, 017202 (2000).
[30] D. D. Berkey, Linear Algebra Appl. **11**, 27 (1975).
[31] In system 2, phases are scaled by 2π, and so they remain between $[0:1]$. After multiplying by 2π they are scattered between $[0:2\pi]$.